OXFORD ◯ FEMS

RESEARCH ARTICLE

Substrate-dependent CO$_2$ fixation in heterotrophic bacteria revealed by stable isotope labelling

Marina Spona-Friedl[1], Alexander Braun[1], Claudia Huber[2],
Wolfgang Eisenreich[2,*], Christian Griebler[1,3], Andreas Kappler[4] and
Martin Elsner[1,5,*,†]

[1]Institute of Groundwater Ecology, Helmholtz Zentrum München, Ingolstädter Landstr. 1, 85764 Neuherberg, Germany, [2]Chair of Biochemistry, Technische Universität München, Lichtenbergstr. 4, 85747 Garching, Germany, [3]Department of Functional and Evolutionary Ecology, Universität Wien, Althanstr. 14, A-1090 Wien, Austria, [4]Geomicrobiology, Eberhard-Karls-University Tuebingen, Sigwartstr. 10, 72076 Tuebingen, Germany and [5]Chair of Analytical Chemistry and Water Chemistry, Technische Universität München, Marchioninistr. 17, 81377 München, Germany

*Corresponding author: Chair of Analytical Chemistry and Water Chemistry, Technische Universität München, Marchioninistr. 17, 81377 München. Tel: +49 89 2180 78231, E-mail: m.elsner@tum.de and Chair of Biochemistry, Technische Universität München, Lichtenbergstr. 4, 85747 Garching, Germany. Tel: +49 89 289 13336, E-mail: wolfgang.eisenreich@mytum.de

One sentence summary: Incorporation of labelled carbon dioxide reveals what type of organic substrate (glucose, lactate, malate) the bacterium *Bacillus subtilis* utilises.

Editor: Lee Kerkhof

†Martin Elsner, http://orcid.org/0000-0003-4746-9052

ABSTRACT

Virtually all heterotrophs incorporate carbon dioxide by anaplerotic fixation. Little explored, however, is the interdependency of pathways and rates of CO$_2$ fixation on the concurrent usage of organic substrate(s). Potentially, this could reveal which substrates out of a pool of dissolved organic carbon are utilised by environmental microorganisms. To explore this possibility, *Bacillus subtilis* W23 was grown in a minimal medium with normalised amounts of either glucose, lactate or malate as only organic substrates, each together with 1 g/L NaH^{13}CO$_3$. Incorporation of H^{13}CO$_3^-$ was traced by elemental analysis-isotope ratio mass spectrometry of biomass and gas chromatography-mass spectrometry of protein-derived amino acids. Until the late logarithmic phase, ^{13}C incorporation into the tricarboxylic acid cycle increased with time and occurred *via* [4–^{13}C]oxaloacetate formed by carboxylation of pyruvate. The levels of ^{13}C incorporation were highest for growth on glucose and lowest on malate. Incorporation of ^{13}C into gluconeogenesis products was mainly detected in the lactate and malate experiment, whereas glucose down-regulated this path. A proof-of-principle study with a natural groundwater community confirmed the ability to determine incorporation from H^{13}CO$_3^-$ by natural communities leading to specific labelling patterns. This underlines the potential of the labelling approach to characterise carbon sources of heterotrophic microorganisms in their natural environments.

Keywords: heterotrophic CO$_2$ fixation; isotope labelling; organic substrate use; dissolved organic matter; bacterial substrate usage; isotope analysis

INTRODUCTION

Reductive carbon fixation under volcanic conditions played a key role in a potential chemoautotrophic origin of life (Huber *et al.* 2012), and CO_2 fixation by autotrophic organisms including plants is among the most important biosynthetic processes in the biosphere (Bassham and Calvin 1962; Giovannoni and Stingl 2005; Berg 2011; Fuchs 2011). However, the presence and diversity of carboxylating (CO_2-fixing) enzymes in nature are not restricted to autotrophs alone. Already 80 years ago, utilisation of CO_2 was reported for heterotrophic bacteria producing propionic acid (*Propionibacteria*) (Wood and Werkman 1936). Today, it is recognised that virtually all heterotrophic organisms—from microorganisms to humans—incorporate CO_2 *via* a variety of pathways involving at least 18 different carboxylases in the central and peripheral metabolism (Dijkhuizen and Harder 1985; Baltar *et al.* 2010; Erb 2011; Middelburg 2011). Among these enzymes, anaplerotic carboxylases incorporate CO_2 into biomass and replenish intermediates of the tricarboxylic acid (TCA) cycle, which are constantly withdrawn for the biosynthesis of amino acids and other metabolic products (Erb 2011). It is therefore not surprising that carbon from anaplerotic CO_2 incorporation accounts for a significant amount (i.e. 2–8%) of the cell's biomass carbon abundance (Romanenko 1964; Perez and Matin 1982; Doronia and Trotsenko 1985; Miltner *et al.* 2004; Roslev *et al.* 2004; Herndl and Reinthaler 2013).

Among the protein family of carboxylases, pyruvate carboxylase, an anaplerotic carboxylase, catalyses the bicarbonate (HCO_3^-)-dependent conversion of pyruvate into oxaloacetate. As a component of a putative ancestral reverse TCA cycle, the enzyme is also present in chemolitho-autotrophic bacteria (Giovannelli *et al.* 2017), which are considered as one of the most ancient forms of life. The reaction of pyruvate carboxylase could therefore represent a metabolic feature that goes back to the early evolution of life (Lombard and Moreira 2011).

The enzyme is widely distributed across the three kingdoms of life and has also been retained in many heterotrophic organisms including the Gram-positive bacterium *Bacillus subtilis* W23. Generally, pyruvate carboxylase occupies a vital position in the central carbon metabolism, since it is located at the 'phosphoenolpyruvate-pyruvate-oxaloacetate node' (Attwood 1995; Owen, Kalhan and Hanson 2002; Jitrapakdee *et al.* 2008). This metabolic hub unites structurally entangled reactions that interconnect the major pathways of carbon metabolism, i.e. glycolysis (catabolism), gluconeogenesis (anabolism) and the TCA cycle (energy supply of the cell) (Sauer and Eikmanns 2005). However, the direction of the carbon fluxes at this metabolic hub (towards catabolism, anabolism or energy supply) primarily depends on the type of the available dissolved organic carbon (DOC) and it can be expected that the amount of incorporated CO_2 (or $^{13}CO_2/H^{13}CO_3^-$ in tracer experiments, respectively) varies even within the same organism depending on the assimilated organic carbon source (Romanenko 1964; Perez and Matin 1982; Doronia and Trotsenko 1985; Miltner *et al.* 2004; Roslev *et al.* 2004). Given a typical metabolic network of a heterotrophic organism capable of carrying out the reaction of pyruvate carboxylase using $H^{13}CO_3^-$ as a substrate, the following simplified scenarios A–C may be distinguished (Fig. 1).

Scenario A: During growth on carbohydrates like glucose (Glc), the glycolytic flux constantly produces pyruvate (Pyr), which is further oxidised to acetyl coenzyme A (Ac-CoA). Ac-CoA requires oxaloacetate (Oxa) to form citric acid (Cit) in the

first reaction of the TCA cycle. The TCA cycle serves, on the one hand, to catabolise substrates to CO_2. On the other hand, intermediates of the TCA cycle are used as building blocks for biosynthesis. Hence, equivalents of Oxa are constantly withdrawn from the TCA cycle for the formation of Asp and related amino acids. Therefore, the pool of Oxa must be replenished to keep the cycle running. To this end, in *B. subtilis* W23, pyruvate carboxylase directly converts Pyr to Oxa *via* the addition of $H^{13}CO_3^-$. Consequently, TCA cycle metabolites and any products derived thereof, e.g. amino acids like Asp, Lys, Thr, Glu or Pro, are expected to carry this label from $H^{13}CO_3^-$.

Scenario B: When substrates such as lactate (Lac) enter the metabolic network somewhere between glycolysis and the TCA cycle, Oxa must also be replenished *via* the reaction catalysed by pyruvate carboxylase, in the same way as in the first scenario. In this case, however, also gluconeogenesis *via* Oxa and phosphoenolpyruvate (PEP) would be expected to become active in order to satisfy the need of the organism for glucose and its derivatives (e.g. for building up membranes and the cell wall of the Gram-positive bacterium). As a result, the ^{13}C-label from $H^{13}CO_3^-$ is expected not only in the metabolites and the products of the TCA cycle (like in the first scenario) but also in those derived from gluconeogenesis or the pentose phosphate pathway, such as Ser, Gly, His, Phe or Tyr.

Scenario C: When cells grow on TCA cycle intermediates like malate (Mal), the substrate directly replenishes the TCA cycle. Hence, Pyr carboxylation seems not to be necessary *per se* and central carbon metabolites are not expected to show ^{13}C incorporation in labelling experiments with $H^{13}CO_3^-$.

However, the assumption that heterotrophic fixation of CO_2/HCO_3^- depends on the organic substrate has not been fully exploited yet. This is surprising since this dependency also has the potential to assign the main carbon source that is utilised by heterotrophic microorganisms. Our study aims to close this gap of knowledge by investigating $H^{13}CO_3^-$ incorporation into *B. subtilis* W23, a well-known model for a heterotrophic bacterium, during growth on glucose, lactate and malate, respectively. These carbon substrates are indicative of the three different entry points to the central carbon metabolism as depicted in the simplified scenarios in Fig. 1. Additionally, these substrates also represent naturally occurring components in soil and DOC (Šantrůčková *et al.* 2005; Kleijn *et al.* 2010; Gleixner 2013).

To assess and to quantify ^{13}C incorporation from $H^{13}CO_3^-$ in our experiments, we used ^{13}C-based metabolic pathway/flux analysis as a key method (Heux *et al.* 2017; Nielsen 2017). Using this technology, carbon from $^{13}CO_2/H^{13}CO_3^-$ can be traced back through the metabolic network of the organism under study. On this basis, not only mechanisms of CO_2 fixation but also downstream fluxes *via* the TCA cycle or gluconeogenesis into metabolic products can be reconstructed on a functional and quantitative basis as shown earlier for plants (Cegelski and Schaefer 2006; Römisch-Margl *et al.* 2007; Schramek *et al.* 2010; Ishihara *et al.* 2015; Bacher, Chen and Eisenreich 2016) or microorganisms (Johnson and Romanenko 1984; Miltner *et al.* 2004; Roslev *et al.* 2004; Hesselsoe *et al.* 2005; Miltner *et al.* 2005; Alonso-Saez *et al.* 2010; Wegener *et al.* 2012). Indeed, the latter experiments also pointed at the crucial role of CO_2 fixation in heterotrophic environmental microbes (Šantrůčková *et al.* 2005; Alonso-Saez *et al.* 2010; DeLorenzo *et al.* 2012; Yakimov *et al.* 2014).

In the present study with *B. subtilis* W23, $H^{13}CO_3^-$-labelling experiments were monitored by elemental analysis-isotope
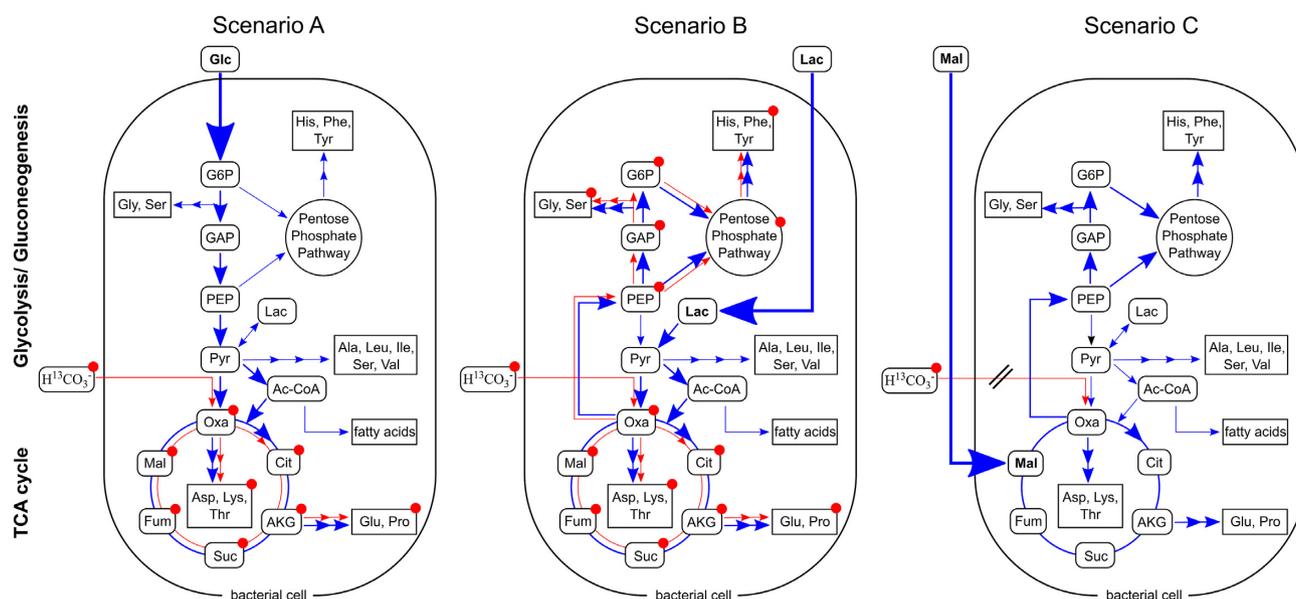
Figure 1. Metabolic routes of ^{13}C-labelled bicarbonate after anaplerotic fixation during growth on different substrates. Scenarios A, B and C show the expected labelling patterns from $H^{13}CO_3^-$ when using unlabelled glucose (Glc), lactate (Lac) or malate (Mal) as main organic carbon substrates. The bold arrows indicate main carbon fluxes. Red arrows show the respective fluxes from the supplied $H^{13}CO_3^-$ tracer through the metabolic network; blue arrows depict the carbon fluxes from the unlabelled organic substrates, respectively. Metabolites and products marked with a red circle are expected to receive ^{13}C-label originating from $H^{13}CO_3^-$.

ratio mass spectrometry (EA-IRMS) of total biomass and by gas chromatography-mass spectrometry (GC-MS) of amino acids to show an example of how to assign main (unlabelled) organic substrates on this basis. Subsequently, $H^{13}CO_3^-$-labelling experiments with a natural microbial community from groundwater were conducted to provide a proof of principle that this approach indeed opens a new avenue to elucidate substrate usages in complex environmental samples.

MATERIALS AND METHODS

Strain and growth conditions

All experiments were performed with *B. subtilis* subsp. *spizizenii* W23 (DSM No.: 6395), a prototrophic derivative of the wild type, obtained from DSMZ (Leibnitz Institute DSMZ—German Collection of Microorganisms and Cell Cultures, Braunschweig, Germany). For pre-cultivation, 5 mL of M9 minimal growth medium, supplemented with 1 g/L glucose, 1 g/L lactate or 1.1 g/L malate, respectively, and preheated to 30°C, were inoculated with 300 μL of a glycerol stock solution of the bacterium. The amounts of organic substrates were chosen in order to ensure that the amount of carbon available to the bacteria (0.4 g/L) was the same in all three set-ups. The pre-cultures were incubated for 20 h. In order to prevent the formation of biofilms, the culture tubes were shaken vigorously at 300 rpm on an orbital incubation shaker (IKA KS 4000i control, IKA-Werke, Staufen, Germany). Each pre-culture was used to inoculate 195 mL of M9 minimal growth medium, preheated to 30°C, in 500 mL Schott bottles. The M9 minimal growth medium was a mixture of 165 mL of M9 minimal medium, 20 mL of a 10 g/L glucose, 10 g/L lactate or 11 g/L malate stock solution, respectively, and 10 mL of a 20 g/L sodium bicarbonate stock solution. The bicarbonate was either $NaH^{13}CO_3$ (98 atom% ^{13}C, Sigma Aldrich, Darmstadt, Germany) in the ^{13}C-labelling experiments or unlabelled $NaHCO_3$ (1.1% natural ^{13}C-abundance, Sigma Aldrich, Darmstadt, Germany) in the control

experiments. The bottles were closed gastight after inoculation to block the release of $^{13}CO_2$. To avoid depletion of O_2, an aliquot of fresh air (filter-sterilised using a 0.22-μm syringe filter) that equals the volume of a taken sample was added at every time point of sampling. The cultivations were performed at 30°C and 150 rpm on an orbital incubation shaker.

The M9 minimal growth medium consisted of the following components (per litre): 8.5 g of $Na_2HPO_4 \cdot 2 H_2O$, 3 g of KH_2PO_4, 1 g of NH_4Cl and 0.5 g of NaCl (= base salts solution). The following components were autoclaved separately before being added to the base salts solution in the given order (per litre): 1 mL of 0.1 M $CaCl_2$, 10 mL trace salts stock solution, 1 mL of 1 M $MgSO_4$ and 1 mL of 50 mM $FeCl_3 \cdot 6 H_2O$ (filter-sterilised using a 0.22-μm syringe filter). The trace salts stock solution contained (per litre): 100 mg of $MnCl_2 \cdot 4 H_2O$, 170 mg of $ZnCl_2$, 43 mg of $CuCl_2 \cdot 2 H_2O$, 60 mg of $CoCl_2 \cdot 6 H_2O$ and 60 mg of $Na_2MoO_4 \cdot 2 H_2O$. The glucose, lactate, malate and sodium bicarbonate stock solutions were filter-sterilised, using a 0.22-μm syringe filter, before being added to the medium. All solutions were prepared using sterilised MilliQ water. All chemicals were purchased from Sigma Aldrich (Darmstadt, Germany).

^{13}C-Labelling experiments and microbial dry weight

Bacillus subtilis subsp. *spizizenii* W23 was grown in M9 minimal growth medium supplemented with 1 g/L glucose, 1 g/L lactate or 1.1 g/L malate, respectively, and 1 g/L sodium bicarbonate. The ^{13}C-labelling experiments were conducted in triplicates and the control experiments with unlabelled bicarbonate in duplicates. After 10 h of incubation, one control experiment was spiked with sodium ^{13}C-bicarbonate (1 g/L); the second control experiment remained untouched. Bacterial growth was monitored by determining the optical density at 600 nm (OD_{600}). Samples for biomass and amino acid analysis were taken at intervals of 2 h after inoculation. At each of these time points, 20 mL of the bacterial culture was harvested by centrifugation

(4°C, 4000 rpm, 20 min). The supernatant was carefully removed, filter-sterilised, using a 0.22-μm syringe filter and stored at –20°C for high performance liquid chromatography (HPLC) analysis (see below). The cell pellet was re-suspended in 2 mL of sterile MilliQ water and transferred into an Eppendorf tube. After this washing step, a second centrifugation step (4°C, 14 000 rpm, 20 min) pelleted the cells again. The supernatant was carefully discarded and the pellet was frozen at –80°C. The frozen pellets were freeze-dried overnight using a VirTis Sentry 8 L benchtop freeze dryer (SP Industries, Warminster, PA, USA). The freeze-dried bacterial pellets were weighed using a high-resolution balance (CP2P, Sartorius AG, Göttingen, Germany) to determine the microbial dry weight.

Testing of the $H^{13}CO_3^-$ method with a microbial groundwater community

Natural oligotrophic and oxic groundwater samples were collected from a shallow unconsolidated quaternary aquifer composed of fluvio-glacial carbonate gravel and sands at Neuherberg/Munich, Germany. The freshly collected groundwater contained 1.5 ± 0.2 mg/L DOC, 1.5 ± 0.15 mg/L nitrate (NO_3^-) and ~15 μg/L phosphate (PO_4^{3-}), whereas the concentrations of nitrite (NO_2^-) and ammonium (NH_4^+) were below the detection limit of ion chromatography (LOD of 0.1 mg/L) (Dionex ICS-1100; Thermo Fisher Scientific, Bremen, Germany): 200 μL of the filter-sterilised samples were analysed to determine the concentrations of the nutrients. A stock solution of an organic fertiliser (DOC content 300 mg/L) was prepared by dissolving the lyophilised substrates at a pH of 9 in ultrapure water, followed by a neutralisation and a centrifugation step. The supernatant was filter-sterilised using a 0.22-μm syringe filter. The organic fertiliser was mainly composed of humic substances of varying molecular size (PhytoGreen®-HumusWP, PhytoSolution, Freyburg, Germany).

Each of two bottles with 400 mL groundwater were loaded with 30 and 50 mL, respectively, of the organic fertiliser, spiked with 1 g/L ^{13}C-sodium bicarbonate (NaH^{13}CO$_3$, 98 atom% ^{13}C, Sigma Aldrich, Darmstadt, Germany) and closed with a screw cap. The bottles were incubated in the dark at room temperature for 52 days (13 September 2018–3 November 2018) and gently mixed once a week. Growth of the bacterial groundwater community was monitored by optical density measurements at 595 nm.

To enhance biomass yield, the two bottles were combined (on 3 November 2018), filled with fresh groundwater to a volume of 1000 mL and supplemented with 25 mL of a soil extract, which was prepared from a dark conifer forest soil by solvent extraction: soil from a coniferous wood was extracted with ultrapure water on a stirrer in darkness at 37°C overnight. The extract was filter-sterilised using a 0.22-μm syringe filter to remove microbes. The DOC content of the sterile soil extract stock solution was 100 mg/L. On 20 December 2018, the bottle was again loaded with 25 mL sterile soil extract. Bacterial growth was monitored by optical density measurements at 595 nm.

The experiment was ended on 18 January 2019 by sacrificing the whole bottle *via* centrifugation. Biomass was concentrated using centrifugal filter units (30 kDa cut-off; Amicon® Ultra-15, Sigma Aldrich, Darmstadt, Germany) to a final volume of 2 mL. The sample was frozen at –80°C and freeze-dried overnight to remove the residual water.

Protein hydrolysis and amino acid derivatisation

For protein hydrolysis, ~0.5 mg of the freeze-dried bacterial pellet was mixed with 500 μL of 6 M hydrochloric acid and heated at 105°C for 24 h. After cooling to 70°C, the residual hydrochloric acid was removed by a constant stream of nitrogen gas. The dried sample was then re-suspended in 50% glacial acetic acid by sonication for 120 s. A small column (1 mL pipet tip) of the cation exchanger Dowex 50WX8 [200–400 mesh (= 37–74 μm), H$^+$ form] was prepared and washed with 1 mL of methanol followed by 1 mL of MilliQ water. After loading the sample onto the column, it was washed twice with 1 mL of MilliQ water. The bound amino acids were then eluted from the column by 1 mL of 4 M ammonium hydroxide. An aliquot of the eluate was dried under a constant stream of nitrogen gas at 70°C. The dry residue was dissolved in 50 μL of water-free acetonitrile and 50 μL of *N*-(tert-butyldimethylsilyl)-*N*-methyl-trifluoroacetamide containing 1% tert-butyldimethylsilylchlorid. This mixture was kept at 70°C for 30 min. The resulting *N*-tert-butyldimethylsilyl derivatives of the amino acids (TBDMS-amino acid derivatives) were analysed by GC-MS following established protocols (Eylert *et al.* 2008).

Gas chromatography/mass spectrometry of silylated amino acids

GC-MS analysis was performed using a 7890A GC system (Agilent Technologies, Santa Clara, CA, USA) equipped with a fused silica capillary column (Equity TM-5; 30 m x 0.25 mm, 0.25-μm film thickness; Supelco, Bellefonte, PA, USA). The mass detector worked with electron impact ionisation at 70 eV. An aliquot (1–3 μL) of the solution containing the TBDMS-amino acid derivatives was injected in a 1:10 split mode. The interface temperature was set to 260°C. The column temperature was held at 140°C for 3 min, heated with a temperature gradient of 4°C/min to 165°C, heated with a second temperature gradient of 15°C/min to 200°C and heated with a third temperature gradient of 7°C/min to 280°C where the temperature was held for 3 min. Selected ion monitoring data were acquired using a 0.3-s sampling rate and the samples were analysed three times. Data collection was carried out *via* the GC-MSD Data Analysis software (Agilent Technologies, Santa Clara, CA, USA). The retention times and the detected mass fragments of the amino acids are listed in Table T1 in the Supporting Information. Incorporation of ^{13}C into amino acids was computed according to Lee *et al.* (1991). The steps include the determination of the contribution of the derivatisation reagent to the observed spectrum of the silylated amino acid and the correction for contribution from ^{13}C-carbon natural abundance using multiple linear regression analysis. The mass isotopomer distribution after this background subtraction provides fractional ^{13}C-excess values for amino acid isotopomers carrying one ^{13}C-carbon atom (M+1), two ^{13}C-carbon atoms (M+2), three ^{13}C-carbon atoms (M+3) and so on, where the sum over all isotopomers [M + (M+1) + (M+2) + (M+3) etc.] is defined as 100%. As an example, amino acids with an M+1 excess value of 50% are composed of 50% unlabelled molecules (M) and 50% molecules carrying one ^{13}C-carbon (M+1) from the ^{13}C-labelled precursor. Amino acids that carry at least one ^{13}C-carbon atom in excess are termed labelled amino acids in the following.

Carbon isotopic analysis of biomass

Carbon isotopic ratios were determined by an elemental analyser-isotope ratio mass spectrometer (EA-IRMS) consisting

of a EuroEA (Euro vector, Milano, Italy) coupled to a Finnigan MAT253 IRMS (Thermo Fisher Scientific, Bremen, Germany) by a Finnigan ConFlow III interface (Thermo Fisher Scientific, Bremen, Germany). For EA-IRMS analysis, a small amount of the freeze-dried pellet (100–400 μg) was put into tin capsules (3.3 × 5 mm; IVA Analysentechnik, Meerbusch, Germany) and subjected to elemental analysis by dropping them into a heated reactor that contained silvered cobalt oxide and chromium oxide (IVA Analysentechnik, Meerbusch, Germany and HEKA tech, Wegberg, Germany). The biomass pellets were combusted in a stream of O_2-containing He at 1000°C to produce N_2, NO_x, H_2O and CO_2, where NO_x was directly converted to N_2 again in an online reduction reactor filled with metallic copper filings. The gases were subsequently transferred to the isotope ratio mass spectrometer *via* a ConFlow III system using a continuous helium stream of 90 mL/min. The CO_2 reference gas was provided by CARBO (Bad Hönningen, Germany). The resulting values from EA-IRMS analysis include the natural abundance of ^{13}C-carbon.

Analysis of substrate consumption (HPLC)

The frozen, filter-sterilised supernatant was used for substrate consumption analysis by HPLC. Briefly, glucose, lactate and malate, respectively, were separated and quantified by HPLC using a ligand exchange Aminex HPX 87H column (300 × 7.8 mm) plus pre-column (30 × 4.6 mm) (Bio-Rad Laboratories GmbH, Feldkirchen, Germany). Aliquots of 20 μL were injected per run. The column oven was set to 40°C. The eluent was 5 mM H_2SO_4 at a flow rate of 0.6 mL/min. Glucose was detected using an RID-10A detector; lactate and malate were detected using the RID-10A and the DAD-SPD-M10Avp detector operating at 210 nm. The retention times of glucose, malate and lactate were 9.1, 9.9 and 12.8 min, respectively.

Statistical analysis

A two-tailed unpaired Student's *t*-test was used for the analysis of differences between the mean values of ^{13}C incorporation into selected pairs of amino acids from the experiments with glucose, lactate and malate. Statistical significance is depicted as ns = not significant, $*P < 0.05$, $**P < 0.01$ or $***P < 0.001$.

RESULTS

Growth of B. *subtilis* in the presence of glucose and $H^{13}CO_3{}^-$

The growth experiment with B. *subtilis* W23 in M9 medium containing glucose and $H^{13}CO_3{}^-$ displayed the usages of both substrates over time for building up its biomass. The glucose concentration in the medium constantly decreased from 5.6 mM to below the analytical detection limit (3 mM in this set-up) at 8 h after inoculation (Fig. 2A). With declining substrate concentration, bacterial biomass increased from 0.03 to 0.44 g/L during the experiment until glucose became limiting. The ^{13}C-abundance of the biomass, as determined by EA-IRMS, steadily rose from 1.1% (natural abundance of ^{13}C-carbon) to a maximum of 6% at 6 h after inoculation (Fig. 2B). Then, the ^{13}C-abundance levelled off and stayed constant at ~5% until the end of the experiment. The control experiment with unlabelled $HCO_3{}^-$ mirrored the natural abundance of ^{13}C-carbon (1.1%) in the environment. In the labelling experiment, the maximum of ^{13}C-abundance of 6% at 6 h and the subsequent decline to 5%
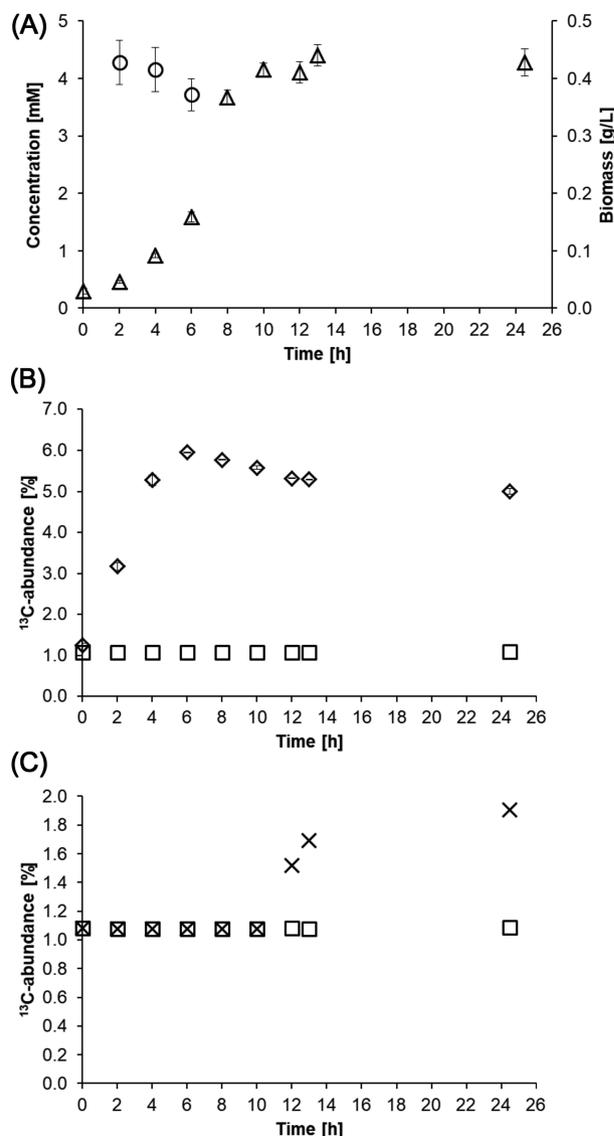
Figure 2. (A) Glucose consumption and biomass production by B. *subtilis* W23 growing in M9 medium containing 1 g/L glucose. The circles represent the glucose concentration and the triangles the biomass production over time. (B) Incorporation of ^{13}C-carbon into microbial biomass by B. *subtilis* W23 growing in M9 medium containing 1 g/L glucose and 1 g/L $NaH^{13}CO_3{}^-$. The diamonds represent the ^{13}C incorporation into the biomass as determined by EA-IRMS measurements. The depicted values are mean values of three biological replicates. The squares represent the control experiment conducted with unlabelled bicarbonate that shows the natural abundance of ^{13}C-carbon of 1.1% in the environment. (C) Incorporation of ^{13}C-carbon into microbial biomass by B. *subtilis* W23 growing in M9 glucose medium containing 1 g/L $NaH^{13}CO_3{}^-$ during the stationary phase. The culture was supplied with the tracer 10 h after inoculation. The ^{13}C-abundance of the biomass (depicted as crosses) increased up to 2%. In a control experiment, no $H^{13}CO_3{}^-$ was added. The ^{13}C-abundance of the biomass (depicted as squares) again mirrored the natural abundance of ^{13}C-carbon in the environment.

could be explained by the production of unlabelled CO_2 *via* respiration of unlabelled glucose, which led to the formation of unlabelled CO_2/bicarbonate in the medium as growth occurred. This production of unlabelled bicarbonate led over time to a dilution of the supplied $H^{13}CO_3{}^-$ as indicated by model calculations (see data files F1–F4 for details and Figure S1 in the Supporting Information). In addition, glucose became limiting so that microbial growth slowed down. Nevertheless, $H^{13}CO_3{}^-$ was still present
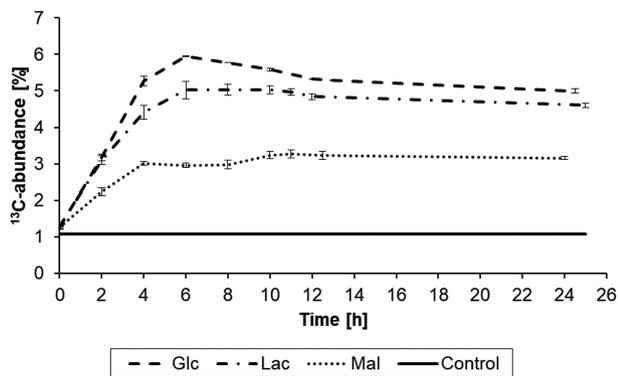
Figure 3. Incorporation of ^{13}C-carbon from H^{13}CO$_3$$^-$ into the biomass of *B. subtilis* W23 growing in M9 containing unlabelled glucose, lactate or malate as carbon sources, respectively. The control shows the natural abundance of ^{13}C-carbon. The depicted values are mean values of three biological replicates. The error bars represent the calculated standard deviation; in case of the control, the error bars are too small to be visible.

in the medium and was used by *B. subtilis* W23 for anaplerosis even during the stationary phase of growth finally leading to a stable ^{13}C-abundance of the bacterial biomass till the end of the experiment (Fig. 2B). Specifically, when ^{13}C-bicarbonate was spiked to a non-labelled control after exponential growth in the stationary phase, i.e. after 10 h of inoculation, the ^{13}C-abundance of the biomass still increased up to ~2% (Fig. 2C). This clearly demonstrated that CO$_2$ fixation took place even in the absence of cell growth indicating active metabolism during the stationary phase. In similar experiments, we added H^{13}CO$_3$$^-$ to *B. subtilis* W23 during the stationary phase when grown on lactate or malate, respectively (see also below). The ^{13}C-abundance of the respective biomass was again determined by EA-IRMS and accounted for 3% in the lactate experiment (Figure S2C, Supporting Information) and 2% in the malate experiment (Figure S3C, Supporting Information). Thus, irrespective of the used carbon substrate and the physiological state (growth phase or stationary phase), metabolic turn-over of oxaloacetate involving the reaction of pyruvate carboxylase remained important, probably to maintain the energy balance also in non-growing *B. subtilis* W23.

Growth of *B. subtilis* in the presence of lactate and H^{13}CO$_3$$^-$

The trends for substrate consumption and biomass production for growth on lactate and H^{13}CO$_3$$^-$ were similar to the experiment with glucose. Briefly, the concentration of lactate decreased from 11.2 to 0.3 mM, while the biomass increased from 0.03 to 0.43 g/L during the experiment (Figure S2A, Supporting Information). Again, the formation of unlabelled bicarbonate caused a dilution of the ^{13}C-label at the end of the experiment. EA-IRMS showed that under these conditions *B. subtilis* W23 incorporated 5% of labelled inorganic carbon into its biomass, which is 1% less compared to the glucose experiment (Figure S2B, Supporting Information) (see also Fig. 3).

Growth of *B. subtilis* in the presence of malate and H^{13}CO$_3$$^-$

In the third experimental set-up, *B. subtilis* W23 was grown in M9 medium supplemented with malate and H^{13}CO$_3$$^-$. Measured substrate consumption demonstrated efficient uptake of

malate (Meyer and Stülke 2013) that was accompanied by an increase of biomass from 0.04 to 0.29 g/L during the experiment. The concentration of malate in the medium decreased from 8.2 mM to below the analytical detection limit of 0.05 mM (Figure S3A, Supporting Information). When using ^{13}C-bicarbonate in the malate medium, the ^{13}C-abundance of the biomass of the bacteria accounted for 3% under these conditions, as measured by EA-IRMS (Figure S3B, Supporting Information). Notably, this value was significantly lower compared to the glucose and lactate experiments (Fig. 3). Nevertheless, the detection of ^{13}C incorporation came as a surprise, since exogenous malate could have fully refilled the TCA cycle without the need for anaplerotic replenishment, introducing the ^{13}C-label (see simplified scenario C in Fig. 1).

^{13}C-Labelling patterns of amino acids

The ^{13}C-EA-IRMS results demonstrated the general importance of heterotrophic CO$_2$ fixation by pyruvate carboxylase. However, the universal label incorporation under different conditions makes it difficult to achieve the primary objective of our study, namely to identify the use of different substrates. In a next step, we therefore focused on amino acid-specific incorporation of ^{13}C, which should provide more specific data concerning substrate usage. As an example, amino acids from the TCA cycle (e.g. Asp, Glu) or gluconeogenesis (e.g. Tyr, Phe) were expected to acquire a greater fraction of ^{13}C-carbon as compared to those amino acids derived from pyruvate (e.g. Val, Ala), where the incorporation of ^{13}C-carbon should be low (see Fig. 1). Using established protocols (Eylert *et al.* 2008), we quantified the ^{13}C-excess (mol%) in 14 amino acids obtained from acidic hydrolysis of the biomass. Among the labelled amino acids, ^{13}C-excess was found especially for isotopomers carrying one ^{13}C-carbon atom (M+1 isotopomers) as expected for a labelling experiment with H^{13}CO$_3$$^-$.

During growth on glucose, ^{13}C-excess of the M+1 isotopomers of amino acids derived from intermediates of the TCA cycle, such as Asp, Thr, Lys, Glu and Pro (see also Fig. 1), reached values up to 50% (Fig. 4A). The ^{13}C-excess of the same isotopomers reached values up to 40% when the bacteria were grown on lactate (Fig. 4B) and values up to 15% during growth on malate (Fig. 4C). The ^{13}C-excess of the M+1 isotopomers of amino acids derived from gluconeogenetic intermediates was low for Ser (~4%) and apparently absent for His (derived from the pentose phosphate pathway intermediate, phosphoribosyl pyrophosphate, PRPP) when *B. subtilis* W23 was grown on glucose, lactate or malate, respectively. Glycine, which is also derived from gluconeogenetic intermediates, showed a moderate ^{13}C-excess of the M+1 isotopomer under all three conditions (6–8%). Amino acids derived from pyruvate such as Ala, Val and Leu received very low ^{13}C-label under all three conditions (<3%). Amino acids (Tyr and Phe) that were synthesised from the pentose phosphate pathway intermediate, erythrose-4-phosphate, showed moderate ^{13}C-excess of the respective M+1 isotopomers (~5%) when *B. subtilis* W23 was grown on lactate or malate (Fig. 4B and C), and no ^{13}C-excess of the same M+1 isotopomers when grown on glucose (Fig. 4A).

From these comparisons, it becomes already evident that the ^{13}C-patterns in amino acids specifically reflected the (unlabelled) organic carbon substrate used by *B. subtilis* W23 in our model experiments. However, to better visualise the differences in the respective substrate usages, we now compared ratios of ^{13}C-excess of the M+1 isotopomers in specific sets of amino acids (Fig. 5). More specifically, Ala and Val were used as rep-

Figure 4. ^{13}C-excess (mol%) of the M+1 isotopers of specific amino acids produced in H^{13}CO$_3{}^-$-labelling experiments with glucose (A), lactate (B) and malate (C), respectively. Amino acids depicted as diamonds are derived from the TCA cycle. Amino acids depicted as circles are derived from pyruvate. Amino acids depicted as crosses are derived from the gluconeogenesis pathway. The ^{13}C-excess of the amino acids derived from pyruvate and the gluconeogenesis pathway are also displayed with a different scaling to improve visibility.

resentatives for ^{13}C incorporation *via* pyruvate (i.e. displaying only very low ^{13}C-excess of the M+1 isotopers in the experimental settings). Tyr and Phe served as representatives for ^{13}C-bicarbonate incorporation *via* gluconeogenesis and the pentose phosphate pathway, whereas Asp and Glu were used as representatives for ^{13}C incorporation *via* the TCA cycle (see also Fig. 1). The ratios of the ^{13}C-excess of the M+1 isotopers at *quasi* steady-state conditions (from 10 h after inoculation till the end of the experiment) gave clear diagnostic trends that uniquely allowed discerning the three different scenarios shown in Fig. 1. When calculating the ratios between the ^{13}C-excess of the M+1 isotopers in TCA cycle-derived amino acids and those of pyruvate-derived amino acids (i.e. Asp/Val, Asp/Ala, Glu/Val and Glu/Ala), values above 20 were obtained in the experi-

iments with glucose or lactate, where TCA cycle metabolites must be replenished, whereas ratios below 10 were obtained for the same sets of amino acids in the experiments with malate, where anaplerosis is not needed (Fig. 5A). When calculating the ratios between the ^{13}C-excess of the M+1 isotopers in gluconeogenesis-derived amino acids and those in pyruvate-derived amino acids (i.e. Tyr/Val, Tyr/Ala, Phe/Val and Phe/Ala), ratios above 4 were obtained for experiments with lactate (i.e. under apparently active gluconeogenesis), whereas ratios of 1 or lower were observed for growth on glucose where gluconeogenesis is not needed (Fig. 5B). Thus, ratios of ^{13}C-excess of the M+1 isotopers between these selected groups of amino acids provided highly selective markers to distinguish the main organic carbon substrates in our model experiments.

Figure 5. Marker ratios of ^{13}C-excess between selected amino acids. (A) ^{13}C-excess (TCA cycle-derived amino acids)/^{13}C-excess (pyruvate-derived amino acids). The coloured bars depict the ratios of the chosen amino acids in three independent labelling experiments with each of the three substrates, glucose (Glc), lactate (Lac) or malate (Mal). The grey bars show the mean values of ^{13}C-ratios for these fractions. The individual ratios as well as the mean values are significantly higher when an active CO_2 fixation is required in the experiments with Glc and Lac compared to a background or random fixation of CO_2 in the experiment with Mal. P-values were calculated by Student's t-test (unpaired): P(Glc/Lac) = 0.05031, P(Glc/Mal) = 0.00003, P(Lac/Mal) = 0.00006. (B) ^{13}C-excess (gluconeogenesis-derived amino acids)/^{13}C-excess (pyruvate-derived amino acids). The coloured bars depict the ratios of the chosen amino acids when glucose or lactate were the growth substrates, respectively, and the grey bars show again the mean values of ^{13}C-ratios. P-value was calculated by Student's t-test (unpaired): P(Glc/Lac) = 0.00017 (for detailed calculation, see the excel file F5 m+1 and ratio of label_SI Paper in the Supporting Information).

Incorporation of ^{13}C-carbon from $H^{13}CO_3^-$ by a natural groundwater community

To test whether this approach can also be used to assign unknown substrates for microbes growing in environmental samples, a proof-of-principle experiment was conducted. Specifically, a natural groundwater microbial community was grown for 124 days in water containing organic fertiliser/soil extract and 1 g/L $H^{13}CO_3^-$ (Fig. 6A and B). Indeed, significant ^{13}C incorporation was found in the biomass of the harvested bacteria (Fig. 6C).

To more specifically assign potential substrates that were used by the microbial community under these conditions, we again analysed amino acids obtained from acidic hydrolysis of the biomass. Overall ^{13}C incorporation and ^{13}C-excess of the M+1 isotopomers were quantified in 16 amino acids. Meso-diaminopimelic acid (DAP, as a component of peptidoglycan) and lysine reached values up to 12% ^{13}C-excess of the M+1 isotopomers (Fig. 6C). These amino acids play important roles

in cell wall biosynthesis of bacteria (Born Timothy and Blanchard 1999). DAP is the immediate precursor for lysine (Lysine biosynthesis—Reference pathway 2020), which explained the similar ^{13}C incorporation into these two amino acids. The detected ^{13}C-label of these amino acids showed (i) ^{13}C incorporation *via* anaplerosis, since DAP and lysine are derived from TCA cycle intermediates and (ii) active cell wall synthesis demonstrating multiplication of the microorganisms under these conditions. Amino acids that are derived from TCA cycle intermediates showed a ^{13}C-excess of the M+1 isotopomers of 3–6%, i.e. Asp (4%), Thr (3%), Met (6%), Glu (4%) and Pro (4%).

To check whether it is possible to reveal the type of organic carbon that has been utilised by the groundwater community, we also calculated the ratios of ^{13}C-excess of the M+1 isotopomers between TCA cycle-derived amino acids and pyruvate-derived amino acids (<10) (Fig. 6D) and the ratios of ^{13}C-excess of the M+1 isotopomers between gluconeogenesis-derived amino acids and pyruvate-derived amino acids (<2) (Fig. 6E). Remarkably, there was a striking similarity between these values and the corresponding values in the model experiments when *B. subtilis* W23 was grown on malate. Consequently, we hypothesise (also with good statistical significance) that the microorganisms from the groundwater community mainly used organic matter that entered the central carbon metabolism at the stage/level of the TCA cycle, like malate. This result seems reasonable since the utilised organic fertiliser was mostly composed of humic substances, i.e. aromatic compounds, which are degraded to compounds comprising four carbon atoms, such as succinyl-CoA and succinate. These products could then serve as main substrates entering the central carbon metabolism *via* the TCA cycle such as malate in our model experiment.

DISCUSSION

By means of anaplerotic CO_2 fixation, *B. subtilis* W23 incorporated ^{13}C-labelled bicarbonate to a different extent into its biomass depending on the main organic carbon source being present in the minimal medium (i.e. glucose, lactate or malate, respectively). Indeed, the data from EA-IRMS analyses alone could already show significant differences between the three carbon substrates tested in this study, as illustrated in Fig. 3. Incorporation of $H^{13}CO_3^-/^{13}CO_2$ to an extent of 6 and 5% into microbial biomass during growth on glucose and lactate, respectively, reflected biomass formation involving anaplerotic carboxylation of pyruvate, which was in some agreement with our simplified scenarios A and B in Fig. 1. Notably, however, in comparison with the glucose experiment, the ^{13}C-abundance of the biomass was lower in the lactate experiment (6 vs 5%). At first glance, this came as a surprise since we expected the same or an even higher ^{13}C-abundance of the bacterial biomass, when lactate was used as the organic substrate. Under lactate conditions, ^{13}C incorporation should also have occurred *via* ^{13}C-labelled oxaloacetate into products derived from intermediates of the TCA cycle as well as into those derived from gluconeogenesis and the pentose phosphate pathway (see scenario B in Fig. 1). The latter routes did not play a major role in the lactate experiment as confirmed by the low levels or the apparent absence of label in His, Ser, Tyr and Phe, respectively. Rather, lactate seemed to be directly channelled *via* pyruvate and Ser into glycerate-3-phosphate and triose phosphates (Glycine, serine and threonine metabolism 2019) and then serving as unlabelled precursors for glucose formation and the pentose phosphate pathway in our experimental setting (Kleijn *et al.* 2010). Following this metabolic flux, cell wall sugars and other gluconeogenetic

Figure 6. Labelling experiment with a natural groundwater community and $H^{13}CO_3^-$ as a tracer. (A) Growth curves of the bacterial groundwater communities growing on different concentrations of organic fertiliser. The microorganisms that were supplemented with 30 mL of organic fertiliser are depicted as open circles. The microorganisms that were supplemented with 50 mL of organic fertiliser are depicted as full circles. **(B) Growth curve of the combined bacterial groundwater community growing on organic fertiliser and soil extract. (C) ^{13}C-excess of the M+1 isotopomers of specific amino acids produced by $H^{13}CO_3^-$-labelling experiments. (D) Marker ratios of ^{13}C-excess between selected amino acids: ^{13}C-excess (TCA cycle-derived amino acids)/^{13}C-excess (pyruvate-derived amino acids).** The coloured bars depict the ratios of the chosen amino acids in the labelling experiments. The grey bars show the mean values of ^{13}C-ratios for these fractions. P-values as calculated by Student's *t*-test (unpaired): P(Glc/Lac) = 0.05031, P(Glc/Mal) = 0.00003, P(Glc/groundwater) = 0.00002, P(Lac/Mal) = 0.00006, P(Lac/groundwater) = 0.00004, P(Mal/groundwater) = 0.00082. **(E) Marker ratios of ^{13}C-excess between selected amino acids: ^{13}C-excess (gluconeogenesis-derived amino acids)/^{13}C-excess (pyruvate-derived amino acids).** The coloured bars depict the ratios of the chosen amino acids in the labelling experiments and the grey bars show again the mean values of ^{13}C-ratios. P-values as calculated by Student's *t*-test (unpaired): P(Glc/Lac) = 0.00017, P(Glc/(Mal) = 0.00002, P(Glc/groundwater) = 0.10712, P(Lac/Mal) = 0.00166, P(Lac/groundwater) = 0.00103, P(Mal/groundwater) = 0.06284.

metabolites would not acquire label from $H^{13}CO_3^-/^{13}CO_2$ *via* ^{13}C-oxaloacetate, thus leading to the observed lower ^{13}C incorporation. Interestingly, transcriptional, translational and post-translational down-regulation of anaplerotic reactions might be triggered by the presence of exogenous organic acids in the medium (Schilling *et al.* 2007; Mirouze *et al.* 2015). Against the background of lactate, as the only organic carbon source in the medium, it seemed safe to assume that anaplerosis was restrained. Similarly, nicotinamide adenine dinucleotide (NADH) in excess produced by lactate dehydrogenase in the presence of lactate would also down-regulate the TCA cycle and its anaplerotic reactions (Cazzulo and Stoppani 1969). Together, less ^{13}C-carbon is incorporated into gluconeogenetic products

and the overall biomass when the bacteria grow on lactate compared to growth on glucose.

The occurrence of the ^{13}C-label in amino acids also clearly assigned pyruvate carboxylase as the $H^{13}CO_3^-/^{13}CO_2$-binding enzyme in all of our settings including the experiment with malate (for details, see below). The unexpected incorporation of 3% ^{13}C-carbon into microbial biomass during growth on malate suggests that, even under this condition, pyruvate carboxylase was still actively transforming pyruvate to oxaloacetate, even though the organism could have directly refilled the oxaloacetate pool of the TCA cycle by taking excess malate from the growth medium (see scenario C in Fig. 1). Thus, although being

characterised as non-essential for *B. subtilis* W23 in SubtiWiki (Zhu and Stülke 2018), the constantly expressed gene for pyruvate carboxylase implies a permanent activity for this enzyme (Sauer and Eikmanns 2005; Jitrapakdee *et al.* 2008)—possibly to be able to quickly react when growth conditions change and anaplerosis becomes necessary for survival (Diesterhaft and Freese 1973; Chubukov *et al.* 2013). Interestingly, metabolic activity of pyruvate carboxylase could also be detected during the stationary growth phase of *B. subtilis* W23 irrespective of the main organic substrate being used from the medium (Fig. 2C; Figures S2C and S3C, Supporting Information). This also indicates the important role of the constantly present enzyme pyruvate carboxylase in the metabolism of *B. subtilis* W23.

EA-IRMS analysis alone could not clearly pinpoint the metabolic history of the incorporated inorganic carbon under the different conditions, nor could it exclude that multiple enzymes contributed to the observed label incorporation. To further confirm that pyruvate carboxylase is responsible for ^{13}C incorporation into microbial biomass and to follow the labelled inorganic carbon through the metabolic network of the microbial cell, we used GC-MS analysis to reveal information about the carbon positions in amino acids having acquired the label. On the basis of the detected fragmentation patterns of the silylated amino acids (for details, see Table T1 in the Supporting Information), some positional assignments of the ^{13}C-label, especially those involving C-1 of the amino acids, were possible (Fig. 7). As an example, the fragments with m/z of 432 and 286 for Glu and Pro, respectively, contained all five carbon atoms of the original amino acid. When analysing the mass spectra, we found that these fragments were accompanied by a high amount (up to 50%) of the respective M+1 isotopomer (namely, m/z 433 for Glu and m/z 287 for Pro). In contrast, the fragments that had lost the C-1 carbon atom of these amino acids (i.e. m/z 404 and 330 for Glu and m/z 258 and 184 for Pro) were not accompanied by a significant excess of the respective M+1 isotopomers (<1%). On this basis, it can be safely concluded that Glu and Pro carried the ^{13}C-label at C-1. Similarly, the mass distribution in the fragments observed for Asp, Thr and Lys signalled high amounts of the respective M+1 isotopomers (up to 50%). Here, the ^{13}C-labelled carbon atom was mainly present at C-4 of these amino acids, as learned from the analysis of the respective fragments. However, lower amounts of ^{13}C-label (1–5%) could also be assigned to C-1 of these amino acids. As illustrated in Fig. 7, this label distribution can be explained because (i) C-4 of oxaloacetate acquires the ^{13}C-label from $H^{13}CO_3^-$ by the reaction of pyruvate carboxylase, (ii) $[4-^{13}C]$oxaloacetate is converted into $[1-^{13}C]\alpha$-ketoglutarate *via* the oxidative branch of the TCA cycle (leading to the detected $[1-^{13}C]$-isotopomers of Glu and Pro), (iii) the biosynthesis of Asp, Thr and Lys is based on the TCA cycle intermediate oxaloacetate (leading to the detected $[4-^{13}C]$-isotopomers) and (iv) reversible reactions between oxaloacetate and succinate, in the reductive branch of the TCA cycle, lead to a scrambling of label between C-1 and C-4 of the symmetric intermediates fumarate and succinate. Hence, the ^{13}C-label was transferred also into C-1 of oxaloacetate and its downstream products Asp, Thr and Lys (see also Fig. 7, red half circles). Remarkably, the position-specific incorporation of ^{13}C-carbon at C-1 of Glu and Pro, and C-4 of Asp, Thr and Lys reached values up to 50% when the bacteria were grown on glucose and as high as 40% when grown on lactate (Fig. 4A and B). These data demonstrated that the anaplerotic reaction catalysed by pyruvate carboxylase transferred the ^{13}C-label efficiently and quite specifically into C-4 of oxaloacetate and its related downstream products (Fig. 7), and, thereby, gave direct evidence of the heterotrophic CO_2 fixation. During growth

on malate, the ^{13}C-label was found at the same positions, but the ^{13}C-excess of the respective M+1 isotopomers was significantly lower (<15%) (Fig. 4C). The amino acids derived from glycolytic precursors, especially Ser and Gly, were characterised by a ^{13}C incorporation at C-1 of 2.8, 3.6 or 4.5% (Ser) and 6.4, 8.8 or 7.7% (Gly), when *B. subtilis* W23 was grown on glucose, lactate or malate, respectively. This ^{13}C incorporation could again be explained by the equilibrium reactions of the TCA cycle: $[4-^{13}C]$oxaloacetate led to $[4-^{13}C]$-isotopomers of malate, fumarate and succinate. Since succinate and fumarate are symmetrical intermediates of the TCA cycle, they led in turn to an equal mixture of $[1-^{13}C]$- and $[4-^{13}C]$oxaloacetate (Fig. 7, red half circles). An active gluconeogenesis could then have transported the ^{13}C-label from the C-1 position of oxaloacetate into the C-1 position of PEP and upstream from there into $[1-^{13}C]$Ser and $[1-^{13}C]$Gly. However, *B. subtilis* W23 could also have used the reversible reaction of the Gly cleavage system (Kikuchi *et al.* 2008) to synthesise Gly, as shown in the following formula.

$$Glycine + H_4folate + NAD^+ \rightleftharpoons N^5, N^{10} - methylene - H_4folate$$
$$+ CO_2 + NH_4^+ + NADH + H^+$$
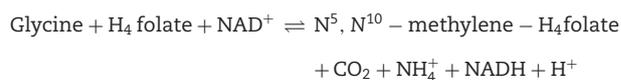
The reverse reaction of the glycine cleavage system could have afforded $[1-^{13}C]$Gly, which then serves as the precursor for Ser biosynthesis yielding $[1-^{13}C]$Ser without the requirement of an active pyruvate carboxylase (Kikuchi *et al.* 2008; Glycine, serine and threonine metabolism 2019). Alternatively, $[1-^{13}C]$Gly could be formed by cleavage of 2-aminoacetoacetate (obtained from Thr) whereby C-1 and C-2 of Thr are transformed into C-1 and C-2 of Gly, respectively. Thus, *via* this route the detected (low) label at C-1 of Thr is transferred to C-1 of Gly. Now, one could speculate that these alternative pathways should be active under all the experimental set-ups and, consequently, the same ^{13}C-excess of the respective M+1 isotopomers of Gly and Ser should have resulted in all three cases. This is not true (Fig. 4) and, therefore, the detected differences in ^{13}C incorporation indicate that a significant fraction of Ser and Gly was synthesised *via* $[1-^{13}C]$-PEP. However, we cannot exclude that different Gly biosynthesis pathways are used by *B. subtilis* W23 when growing on different organic substrates.

In summary, our experiments using $H^{13}CO_3^-$ as a tracer and *B. subtilis* W23 as a model organism, as well as our proof-of-principle experiment with a natural groundwater community, therefore provide solid evidence that EA-IRMS analysis of the biomass in conjunction with GC-MS analysis of protein- and cell wall-derived amino acids (i) reflect the core functional metabolic networks of the organism(s) under study and (ii) can identify the type of the main organic carbon substrate or at least the substrate family being used by the heterotrophic organism or organisms under study.

The general validity of this hypothesis is supported by the fact that almost all heterotrophs need to refill the TCA cycle by anaplerotic CO_2 fixation. For this purpose, heterotrophs use either pyruvate carboxylase that is highly conserved and found in a great variety of organisms, including prokaryotes, archaea, yeasts, fungi and higher organisms (e.g. mammals) or PEP carboxylase, which is also widely distributed in bacteria (Attwood 1995; Jitrapakdee and Wallace 1999; Sauer and Eikmanns 2005; Jitrapakdee *et al.* 2008). PEP carboxylase serves as another anaplerotic enzyme that catalyses the reaction from PEP to oxaloacetate *via* the addition of bicarbonate. Presumably, this results in the same labelling patterns when starting from
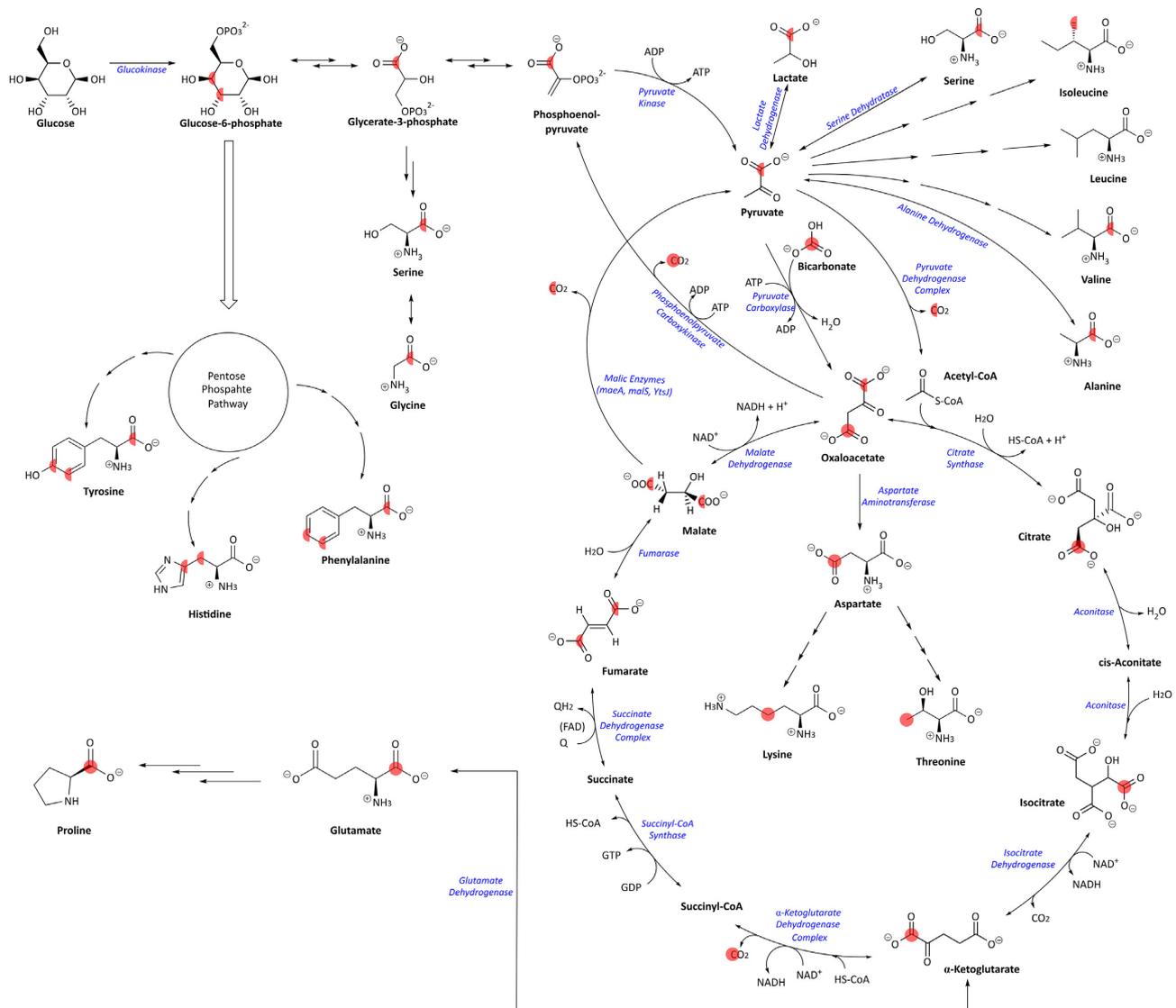
Figure 7. Metabolic network observed for B. subtilis W23 growing in M9 medium containing H^{13}CO$_3^-$ as a tracer. The full red circles mark the location of the ^{13}C-carbon atom detected in amino acids. On this basis, the labelling profiles of their respective precursors were reconstructed. The equilibrium between the reactions of the reductive branch of the TCA cycle could transfer the ^{13}C-label from oxaloacetate to malate, fumarate and succinate. The intrinsic symmetry of fumarate leads to the formation of a 0.5:0.5 mixture of [1–^{13}C]- and [4–^{13}C]malate, and [1–^{13}C]- and [4–^{13}C]oxaloacetate, respectively. This is indicated by the red half circles.

H^{13}CO$_3^-$ in comparison to organisms using the pyruvate carboxylase. Thus, labelling experiments using H^{13}CO$_3^-$ as a tracer bear high potential to generally assign the type of microbial DOC utilisation under various conditions.

SUPPLEMENTARY DATA

Supplementary data are available at FEMSEC online.

FUNDING

ACKNOWLEDGEMENTS

Conflict of interest. None declared.

REFERENCES

Alonso-Saez L, Galand PE, Casamayor EO *et al.* High bicarbonate assimilation in the dark by Arctic bacteria. *ISME J* 2010;**4**:1581–90.

Attwood PV. The structure and the mechanism of action of pyruvate carboxylase. *Int J Biochem Cell Biol* 1995;**27**:231–49.

Bacher A, Chen F, Eisenreich W. Decoding biosynthetic pathways in plants by pulse-chase strategies using $^{13}CO_2$ as a universal tracer. *Metabolites* 2016;**6**:1–24.

Baltar F, Arístegui J, Sintes E *et al*. Significance of non-sinking particulate organic carbon and dark CO_2 fixation to heterotrophic carbon demand in the mesopelagic northeast Atlantic. *Geophys Res Lett* 2010;**37**:1–6.

Bassham JA, Calvin M. The way of CO_2 in plant photosynthesis. *Comp Biochem Physiol* 1962;**4**:187–204.

Berg IA. Ecological aspects of the distribution of different autotrophic CO_2 fixation pathways. *Appl Environ Microbiol* 2011;**77**:1925–36.

Born Timothy L, Blanchard JS. Structure/function studies on enzymes in the diaminopimelate pathway of bacterial cell wall biosynthesis. *Curr Opin Chem Biol* 1999;**3**:607–13.

Cazzulo JJ, Stoppani AO. Effects of adenosine phosphates and nicotinamide nucleotides on pyruvate carboxylase from baker's yeast. *Biochem J* 1969;**112**:755–62.

Cegelski L, Schaefer J. NMR determination of photorespiration in intact leaves using *in vivo* $^{13}CO_2$ labeling. *J Magn Reson* 2006;**178**:1–10.

Chubukov V, Uhr M, Le Chat L *et al*. Transcriptional regulation is insufficient to explain substrate-induced flux changes in *Bacillus subtilis*. *Mol Syst Biol* 2013;**9**:1–13.

DeLorenzo S, Brauer SL, Edgmont CA *et al*. Ubiquitous dissolved inorganic carbon assimilation by marine bacteria in the Pacific Northwest coastal ocean as determined by stable isotope probing. *PLoS One* 2012;**7**:1–15.

Diesterhaft MD, Freese E. Role of pyruvate carboxylase, phosphoenolpyruvate carboxykinase, and malic enzyme during growth and sporulation of *Bacillus subtilis*. *J Biol Chem* 1973;**248**:6062–70.

Dijkhuizen L, Harder W. Microbial metabolism of carbon dioxide. *Comprehensive Biotechnology* 1985;**1**:409–23.

Doronia NV, Trotsenko YA. Levels of carbon dioxide assimilation in bacteria with different pathways of C1 metabolism. *Mikrobiologiya* 1985;**53**:885–9.

Erb TJ. Carboxylases in natural and synthetic microbial pathways. *Appl Environ Microbiol* 2011;**77**:8466–77.

Eylert E, Schär J, Mertins S *et al*. Carbon metabolism of *Listeria monocytogenes* growing inside macrophages. *Mol Microbiol* 2008;**69**:1008–17.

Fuchs G. Alternative pathways of carbon dioxide fixation: insights into the early evolution of life? *Annu Rev Microbiol* 2011;**65**:631–58.

Giovannelli D, Sievert SM, Hügler M *et al*. Insight into the evolution of microbial metabolism from the deep-branching bacterium, *Thermovibrio ammonificans*. *Elife* 2017;**6**:1–31.

Giovannoni SJ, Stingl U. Molecular diversity and ecology of microbial plankton. *Nature* 2005;**437**:343–8.

Gleixner G. Soil organic matter dynamics: a biological perspective derived from the use of compound-specific isotopes studies. *Ecol Res* 2013;**28**:683–95.

Glycine, serine and threonine metabolism - Bacillus subtilis subsp. spizizenii W23 [Internet]. 2019. [cited 26.10.2019]. https://www.kegg.jp/kegg-bin/highlight_pathway?scale=1.0 &map=bss00260&keyword=glycine, (accessed 15 May 2020).

Herndl GJ, Reinthaler T. Microbial control of the dark end of the biological pump. *Nat Geosci* 2013;**6**:718–24.

Hesselsoe M, Nielsen JL, Roslev P *et al*. Isotope labeling and microautoradiography of active heterotrophic bacteria on the basis of assimilation of $^{14}CO_2$. *Appl Environ Microbiol* 2005;**71**:646–55.

Heux S, Berges C, Millard P *et al*. Recent advances in high-throughput ^{13}C-fluxomics. *Curr Opin Biotechnol* 2017;**43**:104–9.

Huber C, Kraus F, Hanzlik M *et al*. Elements of metabolic evolution. *Chemistry* 2012;**18**:2063–80.

Ishihara H, Obata T, Sulpice R *et al*. Quantifying protein synthesis and degradation in Arabidopsis by dynamic $^{13}CO_2$ labeling and analysis of enrichment in individual amino acids in their free pools and in protein. *Plant Physiol* 2015;**168**:74–93.

Jitrapakdee S, St Maurice M, Rayment I *et al*. Structure, mechanism and regulation of pyruvate carboxylase. *Biochem J* 2008;**413**:369–87.

Jitrapakdee S, Wallace JC. Structure, function and regulation of pyruvate carboxylase. *Biochem J* 1999;**340**:1–16.

Johnson BT, Romanenko VI. Xenobiotic perturbation of microbial growth as measured by CO_2 uptake in aquatic heterotrophic bacteria. *J Great Lakes Res* 1984;**10**: 245–50.

Kikuchi G, Motokawa Y, Yoshida T *et al*. Glycine cleavage system: reaction mechanism, physiological significance, and hyperglycinemia. *Proc Jpn Acad Ser B Phys Biol Sci* 2008;**84**:246–63.

Kleijn RJ, Buescher JM, Le Chat L *et al*. Metabolic fluxes during strong carbon catabolite repression by malate in *Bacillus subtilis*. *J Biol Chem*. 2010;**285**:1587–96.

Lee WN, Byerley LO, Bergner EA *et al*. Mass isotopomer analysis: theoretical and practical considerations. *Biol Mass Spectrom* 1991;**20**:451–8.

Lombard J, Moreira D. Early evolution of the biotin-dependent carboxylase family. *BMC Evol Biol* 2011;**11**:1–22.

Lysine biosynthesis - Reference pathway. 2020, . [cited 14.02.2020]. https://www.kegg.jp/kegg-bin/highlight_pathway?scale=1.0&map=map00300&keyword=Diaminopimelate, (accessed 15 May 2020).

Meyer FM, Stülke J. Malate metabolism in *Bacillus subtilis*: distinct roles for three classes of malate-oxidizing enzymes. *FEMS Microbiol Lett* 2013;**339**:17–22.

Middelburg JJ. Chemoautotrophy in the ocean. *Geophy Res Lett* 2011;**38**:1–4.

Miltner A, Kopinke F-D, Kindler R *et al*. Non-phototrophic CO_2 fixation by soil microorganisms. *Plant Soil* 2005;**269**:193–203.

Miltner A, Richnow H-H, Kopinke F-D *et al*. Assimilation of CO_2 by soil microorganisms and transformation into soil organic matter. *Org Geochem* 2004;**35**:1015–24.

Mirouze N, Bidnenko E, Noirot P *et al*. Genome-wide mapping of TnrA-binding sites provides new insights into the TnrA regulon in *Bacillus subtilis*. *Microbiologyopen* 2015;**4**:423–35.

Nielsen J. Systems biology of metabolism. *Annu Rev Biochem* 2017;**86**:245–75.

Owen OE, Kalhan SC, Hanson RW. The key role of anaplerosis and cataplerosis for citric acid cycle function. *J Biol Chem* 2002;**277**:30409–12.

Perez RC, Matin A. Carbon dioxide assimilation by *Thiobacillus novellus* under nutrient-limited mixotrophic conditions. *J Bacteriol* 1982;**150**:46–51.

Romanenko VI. Heterotrophic CO_2 assimilation by water bacterial flora. *Mikrobiologiia* 1964;**33**:679–83.

Roslev P, Larsen MB, Jørgensen D *et al*. Use of heterotrophic CO_2 assimilation as a measure of metabolic activity in planktonic and sessile bacteria. *J Microbiol Methods* 2004;**59**:381–93.

Römisch-Margl W, Schramek N, Radykewicz T *et al*. $^{13}CO_2$ as a universal metabolic tracer in isotopologue perturbation experiments. *Phytochemistry* 2007;**68**:2273–89.

Šantrůčková H, Bird MI, Elhottová D *et al*. Heterotrophic Fixation of CO_2 in Soil. *Microb Ecol* 2005;**49**:218–25.

Sauer U, Eikmanns BJ. The PEP-pyruvate-oxaloacetate node as the switch point for carbon flux distribution in bacteria. *FEMS Microbiol Rev* 2005;**29**:765–94.

Schilling O, Frick O, Herzberg C *et al.* Transcriptional and metabolic responses of *Bacillus subtilis* to the availability of organic acids: transcription regulation is important but not sufficient to account for metabolic adaptation. *Appl Environ Microbiol* 2007;**73**:499–507.

Schramek N, Wang H, Römisch-Margl W *et al.* Artemisinin biosynthesis in growing plants of *Artemisia annua*. A $^{13}CO_2$ study. *Phytochemistry* 2010;**71**:179–87.

Wegener G, Bausch M, Holler T *et al.* Assessing sub-seafloor microbial activity by combined stable isotope probing with deuterated water and ^{13}C-bicarbonate. *Environ Microbiol* 2012;**14**:1517–27.

Wood HG, Werkman CH. The utilisation of CO_2 in the dissimilation of glycerol by the propionic acid bacteria. *Biochem J* 1936;**30**:48–53.

Yakimov MM, La Cono V, Smedile F *et al.* Heterotrophic bicarbonate assimilation is the main process of *de novo* organic carbon synthesis in hadal zone of the Hellenic Trench, the deepest part of Mediterranean Sea. *Environ Microbiol Rep* 2014;**6**:709–22.

Zhu B, Stülke J. SubtiWiki in 2018: from genes and proteins to functional network annotation of the model organism *Bacillus subtilis*. *Nucleic Acids Res* 2018;**46**:743–8.